Innovative Mechanisms for Precision Assembly and Actuation of Arrays of Nanowire Oscillators

Kwanoh Kim,[†] Frank Q. Zhu,[‡] and Donglei Fan[†,§,*]

[†]Department of Mechanical Engineering, the University of Texas at Austin, Austin, Texas 78712, United States, [‡]HGST (formerly Hitachi Global Storage Technologies), 3403 Yerba Buena Road, San Jose, California 95135, United States, and [§]Materials Science and Engineering Program, the University of Texas at Austin, Austin, Texas 78712, United States

ABSTRACT Bottom-up assembling of Micro/Nano Electromechanical System (MEMS/NEMS) devices from nanoscale building blocks is highly desirable but extremely difficult to achieve. In this work, we report innovative mechanisms for precision assembly and actuation of arrays of nanowire NEMS devices that can synchronously oscillate between two designated positions for over 4000 cycles. The assembly and actuation mechanisms are based on unique magnetic interactions between nanoentities with perpendicular magnetic anisotropy (PMA) and electric-tweezer manipulation, our recent invention. Quantitative analysis of the dynamics of torques involved in the nano-oscillators reveals that the induced electrostatic torques due to the external electric fields between metallic NEMS components play a significant role in the mechanical actuation. These new findings are expected to inspire new in situ assembly and actuation strategies in the general field of NEMS devices such as nanomechanical switches for toggling on/off circuits and nanoresonators for biochemical sensors and radio frequency communication.

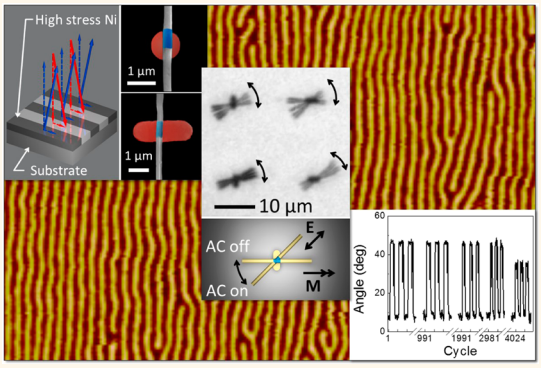

KEYWORDS: NEMS · nano-oscillator · bottom-up assembly · perpendicular magnetic anisotropy · electric tweezers · nanoparticles · nanowires

Nanotechnology has intrigued the research community for over a decade, not just due to the rich fundamental science when materials are made on the nanoscale, but also due to the high potential of making revolutionary impact on critical technologies.[1] Recently, intensive research efforts have focused on using nanoentities as actuation components for Micro/Nano Electromechanical System (MEMS/NEMS) devices owning to the unique advantages that nanotechnology can provide: (1) the size of the MEMS devices can be significantly shrunk with nanoscale building blocks;[2,3] (2) the unique physical/chemical/electrical properties of nanoparticles can improve the performance of miniaturized mechanical devices.[4,5] Various nanomechanical devices with nanoentities as building blocks have been demonstrated including biochemical delivery nanovehicles,[6] chemical and biological sensors,[7−9] mechanical logic gates,[10] nanooscillators,[11,12] nanoswitches,[13,14] mechanical nanorelays,[15] and nanoactuators.[16,17] However, the application of NEMS has been greatly hindered by the arduous nature of top-down lithographical fabrication methods that require advanced skills and elaborate instrumentation, as well as the limited strategies to actuate NEMS.

In this work, we report innovative mechanisms for precision assembly and actuation of arrays of nanowire NEMS devices that can synchronously toggle between two designated positions for over 4000 cycles. The assembling and actuation mechanisms are based on unique magnetic interactions between nanoentities with perpendicular magnetic anisotropy (PMA) and electric-tweezer manipulation, our recent invention. These new mechanisms may be applied to efficient bottom-up assembly of various NEMS devices such as nanomechanical switches for turning on/off nanocircuits and nanoresonators for biochemical sensors and radio frequency communication and are significant

* Address correspondence to dfan@austin.utexas.edu.

Received for review January 23, 2013 and accepted March 13, 2013.

Published online March 13, 2013
10.1021/nn400363x

improvements in terms of efficiency and facility over the commonly used.

Even though substantial advances have been made in the synthesis and characterization of nanowires, it is dreadful to use existing bottom-up assembly technique including contact printing,[18] bubble-blown assembling,[19] flow-assisted assembling,[20,21] dielectrophoresis,[22−29] or magnetic manipulation,[30−32] to accurately assemble, align, or actuate functional NEMS at desirable locations without substantial postprocessing.

Here we leverage a unique magnetic interaction between nanowires and nanomagnets with perpendicular anisotropy, as well as electric-tweezer technique,[2,12] to achieve precisely controlled assembly and actuation of nanowire oscillators. Multisegment Au/Ni/Au nanowires have been transported and assembled on prepatterned arrays of nanomagnets by electric tweezers, a recently invented nanomanipulation technique based on combined electrophoretic and dielectrophoretic forces.[2,12] The magnetic attraction between the Ni segments in the nanowires and Ni layers inside the nanomagnets plays two roles: first, it precisely anchors nanowires on the patterned magnets (also called magnetic nanoanchors); second, it aligns the nanowires in the initialization magnetic treatment direction (idle direction). By applying an AC electric field (*E*-field) along another designated direction, the orientation of nanowires can be toggled between the idle direction and actuation direction of the AC *E*-field. We have observed that ordered arrays of nanowires can synchronously toggle between the two positions on the magnetic nanoanchors for 4000 times, demonstrating the robustness of the assembling and operation mechanism.

RESULTS AND DISCUSSION

Electric tweezers can controllably manipulate nanowires suspended in liquids with a fine degree of control. The working principles of electric tweezers have been described in details elsewhere.[2,12] With electric tweezers, nanoentities can be compelled to transport and align independently in the directions of the DC and AC *E*-field, respectively. The transport speed, depending on the surface charge on the nanowires and DC *E*-field strength, can be as high as 80 μm/s.[33] By applying the *E*-fields in both the *X* and *Y* directions with suitable duration, nanowires can be manipulated along prescribed trajectories in two dimensions with a precision of at least 150 nm.

By combining the magnetic assembly using site specifically patterned nanomagnets and the aforediscussed electric-tweezer manipulation, we have successfully assembled and integrated nanowires (Figure 1a) with predefined structures and patterns. A schematic diagram of the device is shown in Figure 1b. The critical design is an array of nanoanchors with trilayer Cr/Ni/Au films fabricated in the center of a 500 μm gap

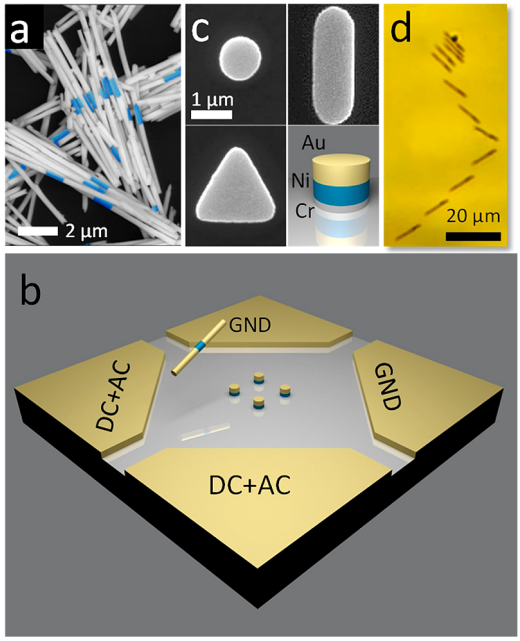

Figure 1. (a) Multisegment Au/Ni/Au nanowires with 1 μm Ni segments in blue. (b) Schematic diagram of electric-tweezer setup consists of Au quadrupole electrodes with a magnetic nanoanchor array at the center. (c) Structure of a Cr/Ni/Au trilayer magnetic nanoanchor and the scanning electron microscopy (SEM) images of the patterned magnetic nanoanchors in shapes of circles, triangles, and rectangles. (d) Overlapped snap shots of a nanowire manipulated by electric tweezers along prescribed trajectories.

quadrupole microelectrode *via* which *E*-fields can be applied. The trilayer anchoring nanomagnets consist of Cr (6 nm) for adherence to the substrate, Ni (100 nm) for providing magnetic forces, and Au (100 nm) for tuning the magnitude of the magnetic forces (Figure 1c). The magnetic nanoanchors were made into various geometries such as circles (1 μm in diameter), bars (1 × 3 μm), and equilateral triangles (2 μm in each side; Figure 1c). The magnetic state of the anchoring nanomagnets were controlled by demagnetization with a gradually reducing oscillating magnetic field of ±10 kG followed by remagnetization with a constant magnetic field of 10 kG applied for 5 s along desirable angles, that is, 0, 45, and 90°. With electric tweezers, nanowires can be transported in the center of the quadrupole electrodes along prescribed trajectories, parallel (AC∥DC) or perpendicular (AC⊥DC) to the transport orientation. When nanowires were positioned in the vicinity of a nanoanchor, they were swiftly attracted to and assembled atop of the nanoanchors, as shown in Figure 1d. Once attached to a nanoanchor, a nanowire cannot be transported by the *E*-fields any longer due to the magnetic attraction. As a result, an array of nanowire assembly can be achieved.

It was also observed that after assembly on the anchors, most of the nanowires aligned in the direction of initial remagnetization of nanoanchors, because the magnetic torque between the nanowires and nanoanchors

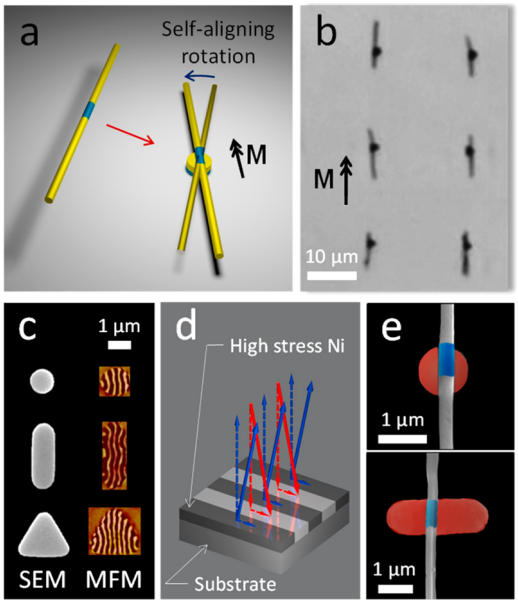

Figure 2. (a) Schematics of self-aligning nanowires. A nanowire approaching at a random angle rotates to the position antiparallel to the magnetization of a magnetic nanoanchor in the direction of M. (b) Au/Ni/Au nanowires assembled on an array of triangle magnetic nanoanchors and aligned parallel to the magnetic orientation. (c) SEM and magnetic force microscopy (MFM) images of magnetic domain structures of magnetic nanoanchors made of stressed Ni thin films. (d) The magnetic orientation of such a unique magnetic material is illustrated. (e) SEM images show precision assembly of nanowires on the magnetic anchors, where the edges of the Ni segments (in blue) flush with the edges of magnetic dots (in red).

caused spontaneous rotation of nanowires to the antiparallel magnetic configuration (Figure 2a and videos S1 and S2 in Supporting Information). Moreover, regardless of how a nanowire approaches a nanoanchor or the geometry of a nanoanchor (circle, bar, or triangle), a nanowire always aligns in the initial remagnetization direction, as shown in Figure 2b. Such a phenomenon cannot be easily explained by the properties of commonly used magnetic materials with a fixed direction of in-plane anisotropy, such as cobalt, iron, or low-rate evaporated nickel. Our investigation shows that the Cr/Ni/Au anchoring nanomagnets have PMA with a small in-plane component that is set along the remagnetization direction. As a result, the magnetic state of Au/Ni/Cr anchoring nanomagnets is controllable and tunable for nanowire assembly along any direction. Characterization with vibrating sampling microscope (VSM) of the Cr/Ni/Au film before patterning showed that its magnetic anisotropy is perpendicular to the film plane, as shown in Figure 3a. Magnetic force microscopy (MFM) images further revealed highly ordered magnetic domain structures in Ni nanopatterns (Figure 2c) after demagnetization in a defined direction. The alternating dark and bright stripes with 120−140 nm periodicity are the magnetic domains with up/down polarities. The line pattern aligns with the direction of in-plane demagnetization field (Figure 2c). This phenomenon is the same as in continuous Ni film. MFM images of continuous Ni film show maze-type domains after perpendicular demagnetization (Figure 3b) and parallel line domain structures after in-plane demagnetization field (Figure 3c). Magneto-restriction due to the high interfacial stresses between Ni and the substrate causes PMA for Ni thin films (evaporated at a high rate >1 Å/s).[34] Different from other magnetic materials with PMA, the PMA of Ni consists of not only a large perpendicular component but also a small in-plane component (Figure 2d), which has been detected by VSM measurement (Figure 3a). The small in-plane magnetic component interacts with Au/Ni/Au nanowire and causes spontaneous alignment of nanowires on the nanoanchor. As shown in Figure 4e, most of the nanowires on nanoanchors align with the magnetic domain direction, regardless of the geometry of the nanomagnet patterns. It indicates that, although the perpendicular polarities of each domain are alternating, which result in an essentially zero net-force on nanowires, the in-plane components have a net moment along one direction, which can attract and align nanowires. Here, *via* the nanowire assembly technique, we directly proved the existence of an in-plane magnetic component in the PMA system of evaporated Ni film, which is often arduous to determine by using traditional magnetic characterization techniques such as VSM and AFM.[35]

The assembly of nanowires with the PMA nanoanchors is so precise that the edges of the Ni segments in the nanowires are flush with the edges of the magnetic nanoanchors. The accuracy of assembly and alignment can be retained even after water evaporation, as shown in Figure 2e. Moreover, we found that the domain alignment of PMA Ni can be readily altered to arbitrary directions and thus the alignment of nanowires can be tailored. Figure 4a−d shows the optical images of assembled nanowires on disk-shaped and bar-shaped magnetic nanoanchors in 2×2 or 2×3 arrays, with the remagnetizing field applied at 0° (a, b) and 45° (c, d). The majority of the nanowires oriented according to the remagnetization direction regardless of the geometry of the nanoanchors. The tunable assembly is achievable *via* facile reorientation of magnetic domain structures by demagnetization + remagnetization along any direction, as shown by MFM images in Figure 4e. As a result, by leveraging the PMA of the nanoanchors, we can accurately and tunably assemble nanowire arrays along desired directions.

The new nanowire assembly strategy by using combined PMA magnetic interaction and electric-tweezer manipulation has great advantages for bottom-up assembly of nanomechanical devices from nanoscale building blocks. For demonstration purposes, we assembled and actuated a 2×2 array of nanowire oscillators, where nanowires synchronously rotate between

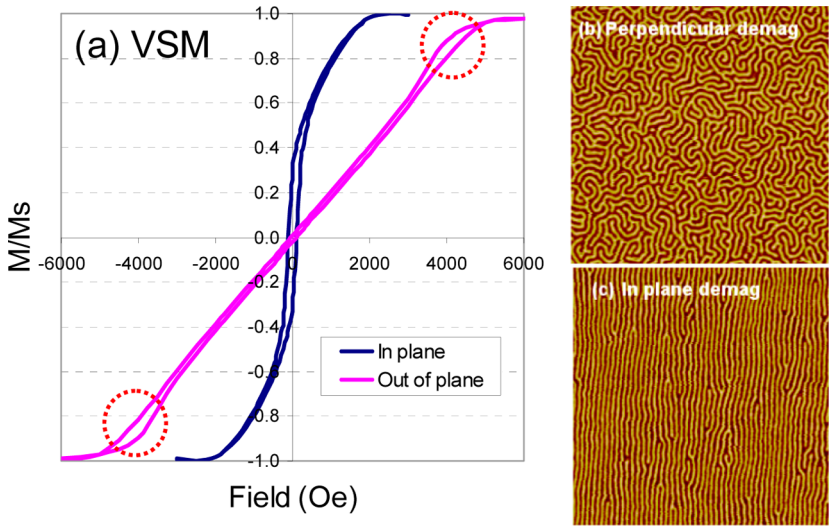

Figure 3. (a) VSM magnetic hysteresis loops of 300 nm thick Ni film measured with in-plane and out-of-plane magnetic fields. Red circles remark the tell-tale sign of perpendicular anisotropy because of the formation of maze domain patterns.[33] (b) MFM image of Ni film after perpendicular demagnetization reveals maze-type magnetic domain pattern and (c) parallel-line domain pattern after in-plane demagnetization. The direction of line domains in (c) is the same as magnetic field direction. Images of (b) and (c) are both 10 × 10 μm^2 in size.

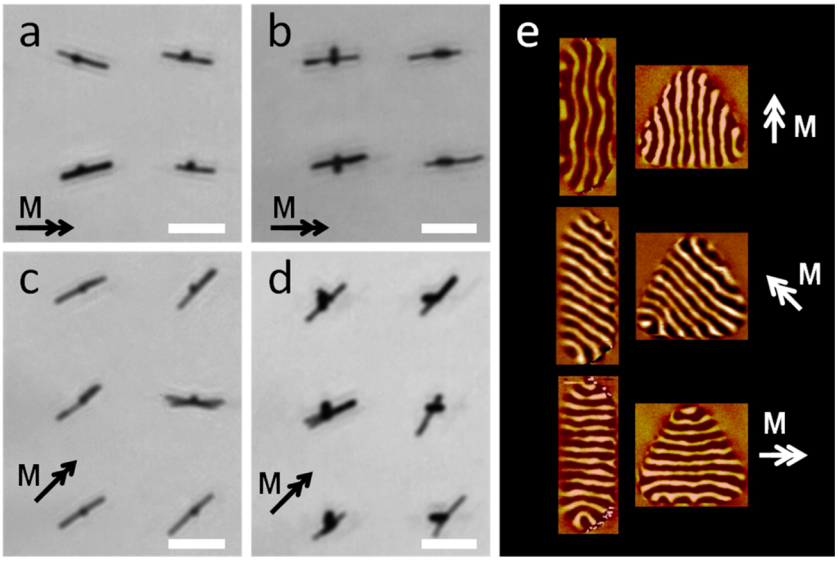

Figure 4. (a–d) Nanowires assembled and aligned on (a, c) disk and (b, d) bar nanoanchors demagnetized along (a, b) 0° and (c, d) 45° (scale bars: 10 μm). (e) Domain wall structures of the bar and triangle nanoanchors demagnetized at 0, 45, and 90°.

two states: aligned in the magnetization direction (**M**) or aligned in the AC *E*-field direction applied at an angle of 90 or 45° relative to **M** (Figure 5a,b and Video S3). The oscillation is achievable by periodically turning the AC *E*-field on and off so that the nanowires align to the AC *E*-field when it is on and restore to the magnetic orientation when it is off. The frequency of oscillation can be controlled by the toggling frequency of the AC *E*-field (Figure 5b). The operation of the nanooscillators is robust and precise. We have recorded 4000 cycles of synchronous rotation before the increased friction at the wire–anchor interface finally stopped the rotation of nanowires (Figure 5c). The contact surface of the nanoanchor endures abrasion when a nanowire oscillates on the nanoanchor. The abrasion of the Au spacer layer reduces the distance x between the magnetic layer in the nanoanchor and the magnetic segment of the nanowire. As a result, the magnetic torque τ_M and the friction torque $\tau_{f,M}$ increase, as they are inversely proportional to x^3 and x^4, given by $\tau_M = (\mu_0(m_1 m_2 \sin\theta_m))/(4\pi x^3)$ and $\tau_{f,M} = (3\ \mu\mu_0(m_1 m_2 \cos\theta_m))/(4\pi x^4)$, respectively ($\mu$, μ_0, m_1, m_2, and θ_m are the coefficient of friction between the nanowire and the nanoanchor, the magnetic constant, the magnetic dipole moments of the nanowire and the nanoanchor, and the angle between the magnetizations of the nanowire and the nanoanchor, respectively). The increment in the torques impedes the motion of nanowire, including oscillation

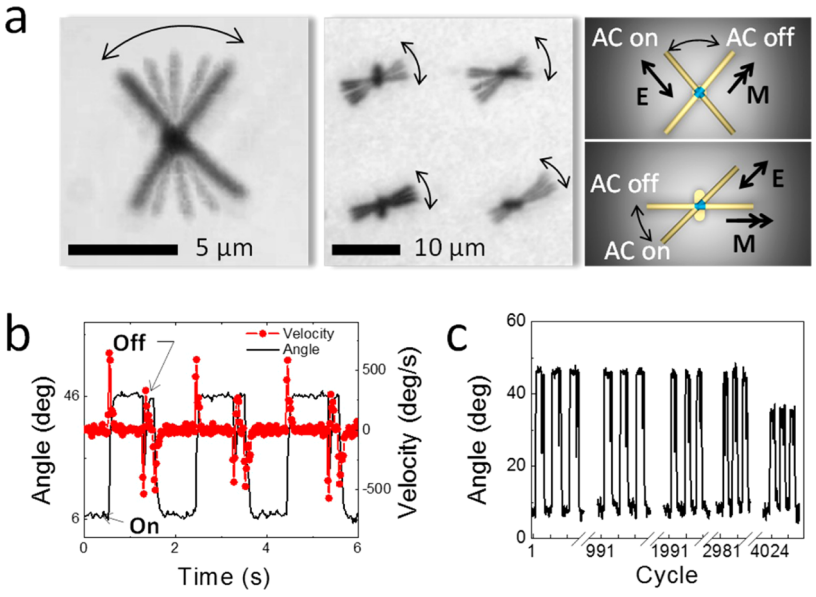

Figure 5. (a) Overlapped snapshots and schematic diagrams of oscillating nanowires assembled on a single disk magnetic nanoanchor and a 2 × 2 array of bar-shaped magnetic anchors. Nanowires rotate between the positions aligning with the external AC *E*-field and aligning with the magnetic orientation of the nanoanchors (M). (b) Angle and angular velocity with respect to time for an oscillating nanowire on a nanoanchor. (c) Robust oscillation of the assembled nanowires for over 4000 cycles.

amplitudes and speeds, under the same external AC *E*-field, and this phenomenon ultimately determines the lifetime of the nanowire oscillator. It was found that the oscillation amplitude significantly reduced after 4000 cycles, and finally, the nanowire was immobilized when the Au layer became too thin and the friction was too high. Currently, we are working on the critical issues of lifetime and frictions in NEMS using innovative lubricants and spacer with much higher hardness.

We have quantitatively calculated the torques exerted on an oscillating nanowire by combining a model and numerical analysis of time-dependent frames captured by a CCD camera. Torques on an oscillating nanowire can be expressed as $\tau_\eta + \tau_e + \tau_M + \tau_{e'} + \tau_f = 0$, where τ_η, τ_e, τ_M, $\tau_{e'}$, and τ_f are liquid drag torque, electrical torque due to external AC *E*-field, magnetic torque, electrical torque due to induced electric polarization of magnetic nanoanchors under external AC *E*-field, and frictional torque, respectively. All the torques are angle-dependent, which makes the calculation complex. But through analysis at extreme angles, when nanowires stop rotation due to balance between the electric ($\tau_e + \tau_{e'}$) and the magnetic (τ_M) torques, we can readily get typical values of electric/magnetic torques involved in the nano-oscillators knowing that the viscous drag (τ_η) and frictional torque (τ_f) can be approximated as zero. With detailed modeling, the comprehensive values of electric, magnetic, frictional, and viscous torques as functions of angle and velocity can be readily determined as shown in Figure 6.

First, the drag torque $\tau_\eta = (-1.74 \times 10^{-19})\ \Omega$ (N·m) is estimated as a function of angular velocity Ω according to the method proposed by Keshoju et al.,[36]

$$\tau_\eta = \frac{1}{3}\Omega\pi\eta l^3 \frac{N^3 - N}{N^3\left[\ln\left(\frac{l}{Nr}\right) + 0.5\right]} = -1.74 \times 10^{-19}\Omega \quad (1)$$

where radius $r = 150$ nm, length $l = 10\ \mu$m for the nanowire, dynamic viscosity $\eta = 0.89 \times 10^{-3}$ Pa for water, and $N = 2$.

The electric torque τ_e by external AC *E*-field can be calculated as below:[37]

$$\tau_e = \frac{8\pi l r^2}{3}\varepsilon_m E^2 (L_y - L_x)\,\mathrm{Re}\left[\frac{(\underline{\varepsilon}_p - \underline{\varepsilon}_m)^2}{[\underline{\varepsilon}_m + (\underline{\varepsilon}_p - \underline{\varepsilon}_m)L_x][\underline{\varepsilon}_m + (\underline{\varepsilon}_p - \underline{\varepsilon}_m)L_y]}\right]\cos 2\theta = B\cos 2\theta \quad (2)$$

where ε_m, $\underline{\varepsilon}_m$, and $\underline{\varepsilon}_p$ are the permittivity of the medium and the complex permittivities of the medium and nanowire, respectively. L_x and L_y are the depolarization factors in the *X* and *Y* directions, respectively. From a free rotating nanowire,[12] the electric torque can be readily measured from the counter drag torque, which is given by $\tau_e = (-1.01 \times 10^{-17}) \cos 2\theta$ (N·m; Figure S4 in Supporting Information). This value is considered to be the same with that of nanowires of the same dimension, material, and fluid medium assembled on nanoanchors.

The magnetic torque τ_M is obtained by analyzing the rotation of a nanowire due to the restoring magnetic torque when the external AC *E*-field is turned off. The rotation is governed by only τ_η, τ_M, and τ_f because τ_e and $\tau_{e'}$ are zeros and τ_M is proportional to sin θ.[38]

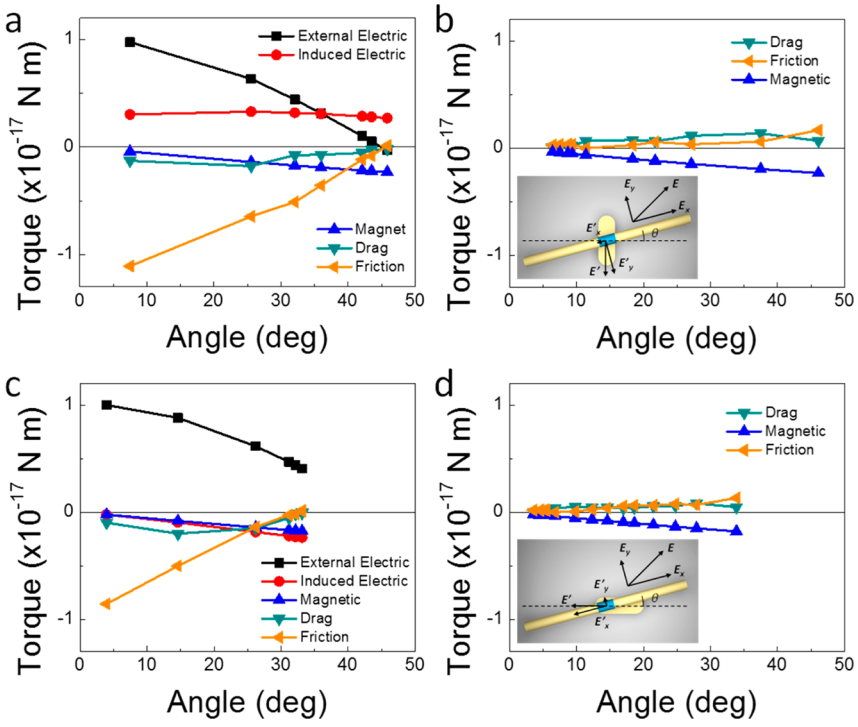

Figure 6. Various torques including electric, magnetic, frictional, viscous, and induced electric torques as functions of angle θ (a, c) with and (b, d) without external AC *E*-fields for a rotating nanowire assembled on a bar magnetic anchor, whose geometric long axis is perpendicular (a, b) or parallel (c, d) to their magnetization orientation.

Therefore, we can readily obtain

$$\tau_\eta = C\sin\theta - \tau_f \quad (3)$$

When the angle θ is small, C and τ_f can be approximated as constant. Then C can be determined from the slope of the τ_η–sin θ curve (Figure S5 in Supporting Information), which results in $\tau_M = (-3.24 \times 10^{-18})$ sin θ (N·m).

We note that the bar-shaped magnetic metal anchors also exert electric torques $\tau_{e'}$ on the nanowires due to the induced dipole moment from the polarization of the external AC *E*-fields. We can estimate such induced electric torque $\tau_{e'}$ on the vertical bar anchor (inset of Figure 6b) from eq 4:[37,39]

$$\tau_{e'\text{vertical}} = D\cos(45^\circ - \theta)\cos\theta \quad (4)$$

where D is a constant and θ is the instantaneous angle of nanowire relative to the horizontal orientation during rotation. The calculation of eq 4 is given in S6. When a nanowire is aligned by the external AC *E*-field and reached a balance at 46°, the induced electric torque can be readily determined from the magnetic torque given by $\tau_{e'} = -(\tau_e + \tau_M)$. Therefore, we obtained $D = 3.86 \times 10^{-18}$. Using a similar approach, we have determined the induced electric torque on the horizontal bar anchor (inset of Figure 6d): $\tau_{e'\ \text{horizontal}} = (-4.42 \times 10^{-18})\cos(45^\circ - \theta)\sin\theta$ (N·m).

Finally, the frictional torque τ_f is given by

$$\tau_f = -(\tau_\eta + \tau_e + \tau_M + \tau_{e'}) \quad (5)$$

where τ_η, τ_e, τ_M, and $\tau_{e'}$ have been calculated as above. The various torques exerted on nanooscillators were plotted as functions of angles in Figure 6 for nanowires rotating on vertical (Figure 6a,b) or horizontal bar-shaped magnetic anchors (Figure 6c,d) when the external *E*-field is on (Figure 6a,c) or off (Figure 6b,d). The torques are in the unit of pN·μm, and the magnitude of the analyzed torques for nanowires rotating on horizontal bar anchors agrees very well with those on vertical bar anchors when the *E*-field is either on or off. We note that the frictional torques τ_f have a noticeable increment when the AC *E*-field is on (Figure 6a,c) than when it is off (Figure 6b,d) in both of the cases of rotating nanowires on a horizontal and a vertical bar. It can be attributed to the increased normal force due to the non-negligible electrostatic attraction between the nanowires and the magnetic anchors under external AC *E*-fields.

Through the analysis of torques involved in the nanooscillators, we quantitatively determined that the induced electrostatic interaction between metallic components in NEMS devices under external AC *E*-field has considerable impact on their mechanical actuation behaviors. The electric torque generated by the induced dipole moment of a magnetic nanoanchor is non-negligible compared to the driving torque of the device: electric torque due to the external AC *E*-field. This is also evidenced by the increased frictional torque due to the strong induced electrostatic interaction between nanowires and nanoanchors when the external

AC *E*-field is on. Moreover, the operation angle of the nanooscillator depends on the relative orientation of the nanowires and bar-shaped nanoanchors, as shown in the insets of Figure 6b,d. As a result, the important effects of the induced electric torques in metallic NEMS devices have been revealed in this work, which is important to consider in making future bottom-up assembled NEMS devices.

CONCLUSION

In summary, we have investigated an innovative scheme for precision assembly and actuation of nanowire nanomechanical devices with combined magnetic interactions and electric tweezers. We studied how the interaction between the PMA nanomagnet anchors and Ni-embedded nanowires resulted in precision assembly, alignment, and actuation of nanowire NEMS devices. The assembly and actuation mechanisms are facile and robust. An array of nano-oscillators has been constructed and synchronously rotated between two defined angular positions up to 4000 cycles. The various complex torques involved in such a system have been analyzed and show excellent consistence between different rotating devices. The important effects of induced electrostatic torques in metallic NEMS were qualitatively revealed. The new approach of *in situ* fabrication and operation of NEMS devices can replace many mechanical fixation structures (such as screws and hinges) and motion recovery parts (such as springs). This research may inspire facile assembling of various NEMS, such as nanoresonators and nanomechanical relays, which is relevant to biochemical sensing and computation, and impact NEMS and nanoelectronics in large.

METHODS

The rotary beams made of three-segment Au/Ni/Au nanowires were fabricated by electrodeposition in anodized aluminum oxide (AAO) template, as reported elsewhere.[12,40] In brief, a 500 nm thick Cu film was evaporated on the backside of an AAO template (nominal pore diameter of 300 nm) and used as a working electrode. Au, Ni, and Au segments were sequentially electroplated into the nanopores. The length of each segment was controlled by the amount of charges passing through the circuit. As a result, arrays of nanowires with 1 μm long Ni segments sandwiched between two 4.5 μm long Au segments were synthesized. After the template was dissolved in a 2 M sodium hydroxide (NaOH) solution, the nanowires were dispersed and centrifuged at least twice in deionized (D.I.) water before resuspended in D.I. water. The backscattered scanning electron microscopic (SEM) image shows the "bamboo" like three-segment nanowires in Figure 1a. Due to the large aspect ratio of the Ni segment, the magnetic easy axis of each Au/Ni/Au nanowire is along the long axis.[38]

Conflict of Interest: The authors declare no competing financial interest.

Acknowledgment. We are grateful for the support of the National Science Foundation CAREER Award (Grant No. CMMI 1150767), Welch Foundation (Grant No. F-1734), and UT-Austin startup package.

Supporting Information Available: Videos of assembling nanowires on nanoanchors with PMA by electric tweezers and their synchronous oscillation in an array. Calculation of the electric, magnetic, and induced electric torques. This material is available free of charge via the Internet at http://pubs.acs.org.

REFERENCES AND NOTES

1. Cao, G.; Wang, Y. *Nanostructures and Nanomaterials: Synthesis, Properties, and Applications*; World Scientific: Singapore; London, 2011.
2. Fan, D. L.; Zhu, F. Q.; Cammarata, R. C.; Chien, C. L. Electric Tweezers. *Nano Today* **2011**, *6*, 339–354.
3. Fan, D. L.; Zhu, F. Q.; Xu, X.; Cammarata, R. C.; Chien, C. L. Electronic Properties of Nanoentities Revealed by Electrically Driven Rotation. *Proc. Natl. Acad. Sci. U.S.A.* **2012**, *109*, 9309–9313.
4. Ekinci, K. L.; Roukes, M. L. Nanoelectromechanical Systems. *Rev. Sci. Instrum.* **2005**, *76*, 061101.
5. Roukes, M. Nanoelectromechanical Systems Face the Future. *Phys. World* **2001**, *14*, 25–31.
6. Fan, D.; Yin, Z.; Cheong, R.; Zhu, F. Q.; Cammarata, R. C.; Chien, C. L.; Levchenko, A. Subcellular-Resolution Delivery of a Cytokine Through Precisely Manipulated Nanowires. *Nat. Nanotechnol.* **2010**, *5*, 545–551.
7. Dan, Y.; Evoy, S.; Johnson, A. T. C. Chemical Gas Sensors Based on Nanowires. *NASA ADS* **2008**, eprint arXiv:0804.4828
8. Cui, Y.; Wei, Q.; Park, H.; Lieber, C. M. Nanowire Nanosensors for Highly Sensitive and Selective Detection of Biological and Chemical Species. *Science* **2001**, *293*, 1289–1292.
9. Ranzoni, A.; Schleipen, J. J. H. B.; van IJzendoorn, L. J.; Prins, M. W. J. Frequency-Selective Rotation of Two-Particle Nanoactuators for Rapid and Sensitive Detection of Biomolecules. *Nano Lett.* **2011**, *11*, 2017–2022.
10. Guerra, D. N.; Bulsara, A. R.; Ditto, W. L.; Sinha, S.; Murali, K.; Mohanty, P. A Noise-Assisted Reprogrammable Nanomechanical Logic Gate. *Nano Lett.* **2010**, *10*, 1168–1171.
11. Weldon, J. A.; Alemán, B.; Sussman, A.; Gannett, W.; Zettl, A. K. Sustained Mechanical Self-Oscillations in Carbon Nanotubes. *Nano Lett.* **2010**, *10*, 1728–1733.
12. Fan, D. L.; Cammarata, R. C.; Chien, C. L. Precision Transport and Assembling of Nanowires in Suspension by Electric Fields. *Appl. Phys. Lett.* **2008**, *92*, 093115.
13. Feng, X. L.; Matheny, M. H.; Zorman, C. A.; Mehregany, M.; Roukes, M. L. Low Voltage Nanoelectromechanical Switches Based on Silicon Carbide Nanowires. *Nano Lett.* **2010**, *10*, 2891–2896.
14. Chen, Z.; Tong, L.; Wu, Z.; Liu, Z. Fabrication of Electromechanical Switch Using Interconnected Single-Walled Carbon Nanotubes. *Appl. Phys. Lett.* **2008**, *92*, 103116.
15. Lee, S. W.; Lee, D. S.; Morjan, R. E.; Jhang, S. H.; Sveningsson, M.; Nerushev, O. A.; Park, Y. W.; Campbell, E. E. B. A Three-Terminal Carbon Nanorelay. *Nano Lett.* **2004**, *4*, 2027–2030.
16. Fennimore, A. M.; Yuzvinsky, T. D.; Han, W.-Q.; Fuhrer, M. S.; Cumings, J.; Zettl, A. Rotational Actuators Based on Carbon Nanotubes. *Nature* **2003**, *424*, 408–410.
17. Marini, M.; Piantanida, L.; Musetti, R.; Bek, A.; Dong, M.; Besenbacher, F.; Lazzarino, M.; Firrao, G. A Revertible, Autonomous, Self-Assembled DNA-Origami Nanoactuator. *Nano Lett.* **2011**, *11*, 5449–5454.
18. Fan, Z.; Ho, J. C.; Jacobson, Z. A.; Yerushalmi, R.; Alley, R. L.; Razavi, H.; Javey, A. Wafer-Scale Assembly of Highly Ordered Semiconductor Nanowire Arrays by Contact Printing. *Nano Lett.* **2008**, *8*, 20–25.
19. Yu, G.; Cao, A.; Lieber, C. M. Large-Area Blown Bubble Films of Aligned Nanowires and Carbon Nanotubes. *Nat. Nanotechnol.* **2007**, *2*, 372–377.

20. Huang, Y.; Duan, X.; Wei, Q.; Lieber, C. M. Directed Assembly of One-Dimensional Nanostructures Into Functional Networks. *Science* **2001**, *291*, 630–633.
21. Huang, Y.; Duan, X.; Lieber, C. M. Nanowires for Integrated Multicolor Nanophotonics. *Small* **2005**, *1*, 142–147.
22. Freer, E. M.; Grachev, O.; Duan, X.; Martin, S.; Stumbo, D. P. High-Yield Self-Limiting Single-Nanowire Assembly with Dielectrophoresis. *Nat. Nanotechnol.* **2010**, *5*, 525–530.
23. Raychaudhuri, S.; Dayeh, S. A.; Wang, D.; Yu, E. T. Precise Semiconductor Nanowire Placement Through Dielectrophoresis. *Nano Lett.* **2009**, *9*, 2260–2266.
24. Li, M.; Bhiladvala, R. B.; Morrow, T. J.; Sioss, J. A.; Lew, K. K.; Redwing, J. M.; Keating, C. D.; Mayer, T. S. Bottom-Up Assembly of Large-Area Nanowire Resonator Arrays. *Nat. Nanotechnol.* **2008**, *3*, 88–92.
25. Vijayaraghavan, A.; Blatt, S.; Weissenberger, D.; Oron-Carl, M.; Hennrich, F.; Gerthsen, D.; Hahn, H.; Krupke, R. Ultra-Large-Scale Directed Assembly of Single-Walled Carbon Nanotube Devices. *Nano Lett.* **2007**, *7*, 1556–1560.
26. Liu, Y.; Chung, J.-H.; Liu, W. K.; Ruoff, R. S. Dielectrophoretic Assembly of Nanowires. *J. Phys. Chem. B* **2006**, *110*, 14098–14106.
27. Harnack, O.; Pacholski, C.; Weller, H.; Yasuda, A.; Wessels, J. M. Rectifying Behavior of Electrically Aligned ZnO Nanorods. *Nano Lett.* **2003**, *3*, 1097–1101.
28. Smith, P. A.; Nordquist, C. D.; Jackson, T. N.; Mayer, T. S.; Martin, B. R.; Mbindyo, J.; Mallouk, T. E. Electric-Field Assisted Assembly and Alignment of Metallic Nanowires. *Appl. Phys. Lett.* **2000**, *77*, 1399–1401.
29. Duan, X.; Huang, Y.; Cui, Y.; Wang, J.; Lieber, C. M. Indium Phosphide Nanowires as Building Blocks for Nanoscale Electronic and Optoelectronic Devices. *Nature* **2001**, *409*, 66–69.
30. Liu, M.; Lagdani, J.; Imrane, H.; Pettiford, C.; Lou, J.; Yoon, S.; Harris, V. G.; Vittoria, C.; Sun, N. X. Self-Assembled Magnetic Nanowire Arrays. *Appl. Phys. Lett.* **2007**, *90*, 103105.
31. Hangarter, C. M.; Myung, N. V. Magnetic Alignment of Nanowires. *Chem. Mater.* **2005**, *17*, 1320–1324.
32. Bentley, A. K.; Trethewey, J. S.; Ellis, A. B.; Crone, W. C. Magnetic Manipulation of Copper−Tin Nanowires Capped with Nickel Ends. *Nano Lett.* **2004**, *4*, 487–490.
33. Xu, X.; Kim, K.; Li, H.; Fan, D. L. Ordered Arrays of Raman Nanosensors for Ultrasensitive and Location Predictable Biochemical Detection. *Adv. Mater.* **2012**, *24*, 5457–5463.
34. Lee, S. H.; Zhu, F. Q.; Chien, C. L.; Marković, N. Effect of Geometry on Magnetic Domain Structure in Ni Wires with Perpendicular Anisotropy: a Magnetic Force Microscopy Study. *Phys. Rev. B* **2008**, *77*, 132408.
35. Zhu, L. Y.; Chen, T. Y.; Chien, C. L. Altering the Superconductor Transition Temperature by Domain-Wall Arrangements in Hybrid Ferromagnet-Superconductor Structures. *Phys. Rev. Lett.* **2008**, *101*, 017004.
36. Keshoju, K.; Xing, H.; Sun, L. Magnetic Field Driven Nanowire Rotation in Suspension. *Appl. Phys. Lett.* **2007**, *91*, 123114.
37. Jones, T. B. *Electromechanics of Particles*; Cambridge University Press: New York, 2005.
38. Coey, J. M. D. *Magnetism and Magnetic Materials*; Cambridge University Press: New York, 2010.
39. Ibach, H.; Lüth, H. *Solid-State Physics: an Introduction to Principles of Materials Science*; Springer: New York, 2009.
40. Whitney, T. M.; Jiang, J. S.; Searson, P. C.; Chien, C. L. Fabrication and Magnetic Properties of Arrays of Metallic Nanowires. *Science* **1993**, *261*, 1316–1319.